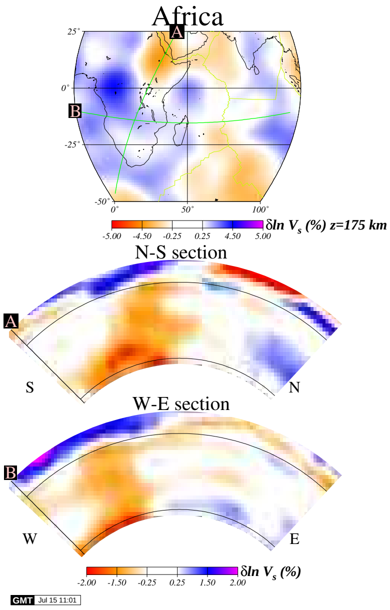

Figure 11.7: West Pacific cross-sections

4.2.2 Slow anomalies

The model presents three large scale slow anomalies that extend continuously from the bottom of the mantle into the uppermost mantle, one under Africa and two in the Pacific. In figure 11.8, we show an image of the upwelling beneath the African continent.

Figure 11.8 (top) shows a lateral section of the upper mantle at 175 km depth under Africa and the Indian Ocean, displaying fast anomalies beneath the African and Indian plates and slow anomalies near the East African rift zone, the Red Sea and along the mid-Indian ridge. The East African, West African and Congo cratons are isolated by the presence of slow regions surrounding them.

Figure 11.8 (A), shows a SW-NE cross-section across the continent. The slow domain under Africa extends vertically from the base of the mantle into the upper mantle and is subsequently shifted to the northeast. The upper mantle image is consistent with the closure of the Tethys by the African continent throughout the Cretaceous: in our tomographic model, the upper part of the low velocity anomaly is offset in the direction of motion of the African plate. Figure 11.8 (B) shows an East-West cross-section. The low velocity zone is deflected to the east by the Nubian plate where it connects with the mid-Indian ridge. In the lower mantle, the shape of the anomaly in *SAW24B16* is in general agreement with the model *M2* of *Ritsema et al*, 1998, suggesting an upwelling shifting in the northeast direction with increasing radius. However, in contrast with their study, we find continuity of the slow domain into the upper mantle.

4.3 Conclusion

This study shows that, with a relatively restrained data set consisting of waveforms of all the phases present on a seismogram, it is possible to derive global images of the mantle on scale lengths of 7.5°, consistent with results of regional studies. This is related to the adoption of a waveform methodology to image deep Earth structure. We use a theoretical formalism valid both for body and surface waves that allows 1) the modeling of finite frequency effects on the seismogram and 2) the use of all the information on the seismic trace. In particular we make use of the S phase diffracted on the core-mantle boundary which cannot be modeled with a ray-theoretic approach and which provides the bulk of lower mantle information; we also use simultaneous phase arrivals which are precluded by travel time studies as they rely on the the determination of an onset time for each datum. This methodology is well suited to the imaging of both fast and slow domains in the earth. The present model suggests the existence of three large scale plume-like slow anomalies in the mantle, one under Africa, and two in the Pacific.

4.4 References

Fukao, Y., M. Obayashi, H. Inoue, and M. Nenbai, Subducting slabs stagnant in the mantle transition zone, *J. Geophys. Res.*, 97, 4,809-4,822, 1992.

Fischer, K. M., K. C. Creager, and T. H Jordan, Mapping the Tonga slab, *J. Geophys. Res.*, 96, 14,403-14,427, 1991.

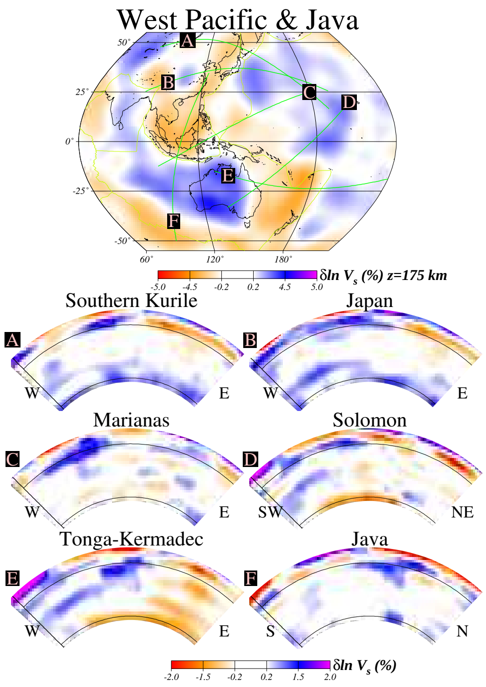

Figure 11.8: Cross-sections through Africa

Li, X.D. and B. Romanowicz, Comparison of global waveform inversions with and without considering cross-branch modal coupling, *Geophys. J. Int., 121,* 695-709, 1995.

Li, X.D. and B. Romanowicz, Global mantle shear-velocity model developed using nonlinear asymptotic coupling theory, *Geophys. J. R. Astr. Soc., 101*, 22,245-22,272, 1996.

Mégnin, C. and B. Romanowicz, The effects of the theoretical formalism and data selection on mantle models derived from waveform tomography, *Geophys. J. Int.*, 138, 366-380, 1999.

Ritsema, J., S. Ni, D. V. Helmberger, and H. P Crotwell, Evidence for strong shear velocity reductions and velocity gradients in the lower mantle beneath Africa, *Geophys. Res. Lett.*, 25, No 23, 4,245-4,248, 1998.

Tajima, F., Y. Fukao, M. Obayashi, and T. Sakurai, Evaluation of slab images in the Northwestern Pacific, *Earth Planets Space*, 50, 953-964, 1998.

van der Hilst, R. D., E. R. Engdahl, W. Spakman, and G. Nolet, Tomographic imaging of subducted lithosphere below northwest pacific island arcs, *Nature*, 353, 37–42, 1991.

5. Inversion of Normal Mode Spectra for Mantle Structure

Chaincy Kuo and Barbara Romanowicz

5.1 Introduction

Observations of the Earth's free oscillations have been a valuable complement to seismic body and surface wave data in constraining materi al properties and their lateral variations in the deep Earth. Most normal mode inversions are cast in terms of a two-step formalism, in which "splitting functions" (*Woodhouse et al., 1986*) are first computed for each mode in the data set. In the second step, splitting functions are simultaneously inverted for the distribution of elastic parameters with depth.

While mantle mode data, in principle, provide information on the Vs, Vp and ρ in the mantle, the sensitivity to Vs is dominant, and most studies to-date have assumed an a-priori scaling between the 3 elastic parameters, and inverted for Vs alone (*Giardini et al., 1987; Li et al., 1991; Resovsky and Ritzwoller, 1998*). In particular, the density structure is thought to be rather poorly resolved.

Following *Li et al (1991)*, and *Durek and Romanowicz (1999)*, we have opted for a direct, one step method, which inverts normal mode spectra directly for 3D earth structure. While more time consuming, this approach is more internally consistent. Using this approach, we have performed inversions in which we simultaneously solve for Vs, Vp, ρ structure up to degree 4 in the mantle, for both even and odd degrees. Our models are radially parameterized up to order 7 in Legendre polynomials.

5.2 Velocity and Density Mantle models

We analyze the vertical component spectra of spheroidal mantle modes whose eigenfunctions primarily exhibit particle motion in the mantle (${}_0S$, ${}_1S$, ${}_2S$, ${}_4S$, ${}_5S$ branches). Modes with significant displacement in the core are not included in this study, although some mantle modes in our data set have some sensitivity to outer core structure. The effect of outer core sensitivity on our models of mantle structure is minimal, and this is consistent with conclusions of *Giardini et al. 1987*. Below 5 mHz, the mantle modes in our study are well-isolated in frequency, which minimizes contamination by neighboring modes. On the other hand, our analysis code is capable of taking into account the more complex effects of 3-D structure on the spectra of coupled mode pairs. In total, we have chosen 30 isolated mantle modes and 7 coupled mantle mode pairs, amounting to a total of 44 spheroidal mantle modes, and a total of 2630 individual spectra.

A variance reduction of 71.4% is obtained after 3 iterations of the non-linear inversion from spectra for our model of mantle structure, *PSR.CP.cmb*. Although we only retrieve very large scale features of lateral heterogeneity in degree 4, there is, in general, good correspondence with expected features of the dynamic Earth, as documented in other studies. Low velocity features in the upper mantle correspond to regions of back-arc basins, and spreading ridges. Fast anomalies are associated with regions of subduction, particularly in the Western Pacific and become prominent under South America at 650 km depth. At the bottom of the mantle, both shear and compressional wave velocity maps exhibit high velocity rings around a low velocity Pacific Ocean (Figure 11.9).

Although our confidence in the retrieval of density structure is marginal, as discussed in a previous section, the density structure retrieved from *PSR.CP.cmb* is not unreasonable: patterns of high density anomalies in the mantle correspond to regions of down-going slabs in the mantle. High density features are present southwest of South America and Western Pacific starting at about 250 km depth, in particular near the Tonga Trench. These features surrounding the Pacific extend all the way down to the base of the mantle (Figure 11.10).

5.3 Geoid Predictions

Many authors have computed geoid predictions from forward-modelled mantle density heterogeneity by simulating the history of slab subduction in the mantle (*Hager, 1984; Ricard et al., 1993; Lithgow-Bertelloni and Richards, 1998*) based on plate motion reconstruction extending to ~180 Ma. The predictions of the geoid from these slab models agree with the observations extremely well. We note that the visual correlation of our mantle density structure with that of *Lithgow-Bertelloni and Richards (1998)* truncated to degree 4 is quite satisfying.

We also can make an independent prediction of the Earth's gravitational potential at the surface from our density model and compare it with the observed geoid to assess further our ability to model density. To fit the degrees 2-6 geoid anomaly, we have used a density model inverted up to degree 6. The observed and synthetic geoid are displayed in Figure 11.11 and include degrees

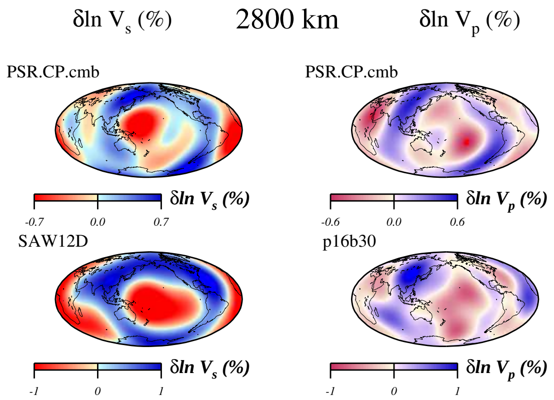

Figure 11.9: At 2800 km, both shear and compressional velocity perturbations exhibit high velocity regions around a slow Pacific. The normal mode spectra derived models are shown at the top (left: δlnV_s, right: δlnV_p, and models from time-domain data are shown at the bottom for comparison (left: SAW12D [*Li and Romanowicz, 1996*], right: p16b30 [*Masters et al., 1996*]).

2-6. It is apparent that the correspondence between the observed and predicted geoid is quite good from visual inspection. In general, the pattern of positive and negative geoid anomalies agree, and there is also a strong agreement in the amplitudes.

5.4 References

Durek, J. and B. Romanowicz, Inner core anisotropy inferred by direct inversion of normal mode spectra, In press, *Geophys. J. Int.*, 1999.

Giardini, D., X.-D. Li, and J.H. Woodhouse, Three-dimensional structure of the Earth from splitting in free-oscillation spectra, *Nature*, **325**, 405-11, 1987.

Hager, B.H., Subducted slabs and the geoid: constraints on mantle rheology and flow. *J. Geophys. Res.*, **89**, 6003-15, 1984.

Li, X.-D., D. Giardini, and J.H. Woodhouse, Large-scale three-dimensional even-degree structure of the Earth from splitting of long-period normal modes, *J. Geophys. Res.*, **96**, 551-77, 1991.

Li, X.-D. and B. Romanowicz, Global mantle shear velocity model developed using nonlinear asymptotic coupling theory. *J. Geophys. Res.*, **101**, 22245-72, 1996.

Lithgow-Bertelloni, C. and M.A. Richards, The dynamics of Cenozoic and Mesozoic plate motions, *Reviews of Geophysics*, **36**, 27-78, 1998.

Masters, G., S. Johnson, G. Laske, and H. Bolton, A shear-velocity model of the mantle. *Philos. Trans. R. Soc. London A*, **354**, 1385-411, 1996.

Resovsky, J.S. and M.H. Ritzwoller, New and refined constraints on three-dimensional Earth structure from normal modes below 3 mHz, *J. Geophys. Res.*, **103**, 783-810, 1998.

Woodhouse, J.H., D. Giardini, and X.-D. Li, Evidence for inner core anisotropy from free oscillations, *Geophys. Res. Lett.*, **13**, 1549-52, 1986.

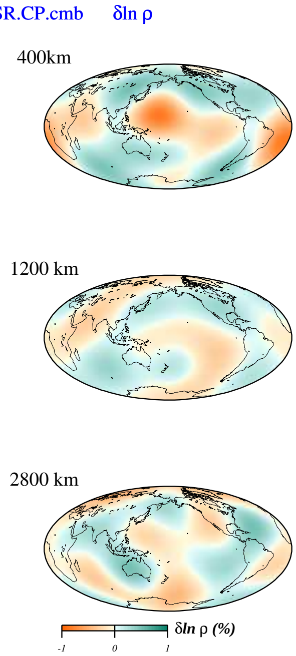

Figure 11.10: Density perturbations at three depths in the mantle

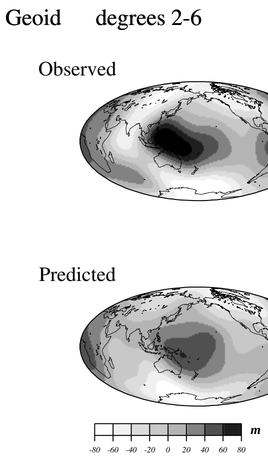

Figure 11.11: Top map: the observed geoid for degrees 2-6, and bottom map: a geoid prediction from a density model derived from normal mode spectra. Dark regions indicate high geoid anomaly, and light regions indicate low geoid anomaly. The scale is ±80 m.

6. Seismological Study of the Upper Mantle Transition Zone Using Broadband Waveform Modeling

Fumiko Tajima

6.1 Anomalous P Wave Speed Models M2.0 and M3.11

Several well-known tomographic studies published in the 1990's (van der Hilst et al., 1991; Fukao et al., 1992) captured a large-scale subhorizontal high velocity anomaly at the bottom of the upper mantle in the northwestern Pacific. These models suggest that a large volume of subducted slab is stagnant in the transition zone. To support the hypothesis, there are also some observational studies for depression of the 660 km discontinuity due to the effects of stagnant cold slab in the same region (Shearer and Masters, 1992; Tajima and Grand, 1995).

Using broadband waveform modeling P wave speed model M3.11 was derived for the transition zone associated with the southern Kurile subduction zone where a large volume of stagnant slab may exist. This model is characterized by a high speed anomaly (relative to a standard model iasp91) below 525 km with its maximum intensity not immediately above the 660 km discontinuity but in a depth range ~100 km above it. On the other hand the transition zone structure beneath the northern Philippine Sea Plate is represented by model M2.0 which has high speed anomaly in the deeper part of the transition zone like M3.11 but with little apparent change in the depth of the 660 km discontinuity (see the agreement between the observed and synthetic waveforms calculated with the optimal models in Figure 11.12). The lack of depression of the discontinuity depth may suggest that the temperature beneath the flattened slab in this area is normal.

An interesting finding is that whether the discontinuity depth is depressed or not, the P wave speed at the phase transition depth is about the same. Models M3.11 and M2.0 in the depth range from ~525 to 660 km are remarkably similar to the P wave speed model derived from bulk moduli measured under high pressure and temperature using a pyrolite composition (Li et al., 1998). Both of the seismic models and the pyrolite model have smaller gradient of P wave speed in the transition zone than iasp91 and converge to the standard model right above the "660" discontinuity.

6.2 Evaluation of Slab Images in the northwestern Pacific

The P wave travel-time tomographic images (Obayashi et al., 1997) were examined using waveform modeling which incorporate the travel-time data of secondary waves. Here note that most P wave tomography experiments do not use travel-time data of secondary waves. Those secondary waves are highly sensitive to the velocity structure above the 660 km discontinuity and thus add information on the seismic structure of the transition zone independent of that used in many tomography experiments. Our results show strong variations in the transition zone structure beneath the northwestern Pacific. The overall results are in agreement with past work indicating fairly broad regions where the subducting plate is lying flat or piling up within the transition zone, although we find that the region where this occurs, and thus the total volume of slab within the upper mantle, is considerably less than that seen in past studies (Tajima and Grand, 1998). Results also suggest that the anomalous structure associated with a stagnant slab has its maximum intensity not immediately above the 660 km discontinuity but in the depth range ~100 km above it (Tajima et al., 1998) (see the cross projection profiles of the tomographic images by Obayashi et al. (1997) and the overlain seismic rays for which M3.11 is a suitable model in Figure 11.13).

6.3 References

Fukao, Y., M. Obayashi, H. Inoue, and M. Nenbai, Subducting slabs stagnant in the mantle transition zone, J. Geophys. Res., 97, 4809-4822, 1922.

Li, B., R. C. Liebermann, and D. J. Weidner, Elastic moduli of waldsleyite (β-Mg_2SiO_4) to 7 Gigapasscals and 873 Kelvin, Science, 281, 675-677, 1998.

Shearer, P.M., and T. G. Masters, Global mapping of topography on the 660-km discontinuity, Nature, 355, 791-796, 1992.

Tajima, F., and S. P. Grand, Evidence of high velocity anomalies in the transition zone associated with southern Kurile subduction zone, Geophys. Res. Lett., 22, 3139-3142, 1995.

Tajima, F., and S. P. Grand, Variation of transi-

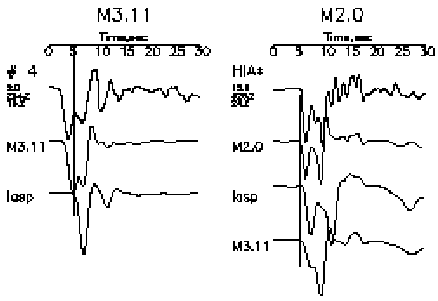

Figure 11.12: P waveforms observed at HIA station in China for events from the southern Kurile (left) and Izu-Bonin (right) subduction zones (top bold traces) and synthetics which are modeled well by M3.11 or M2.0, respectively (thin traces immediately below the observed waves). Below those are the synthetics with other models (iasp for iasp91) for comparison.

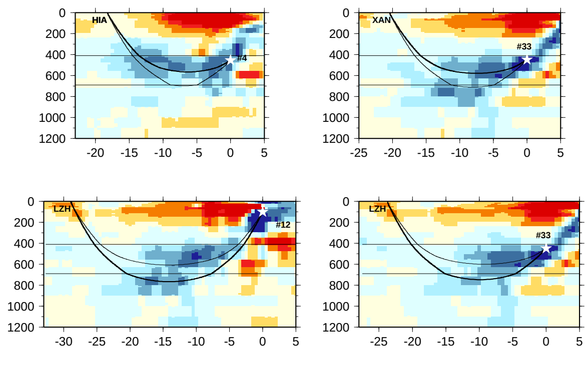

Figure 11.13: Cross projection profiles of slowness along some of the ray paths for the preferred model of M3.11. The peak of high velocity anomalies in the depth range 478-551 km in the tomographic model, but the agreement between the tomographic image and the waveform modeling is reasonable along these profiles.

tion zone high velocity anomalies and depression of the "660"km discontinuity associated with subduction zones from the southern Kuriles to Izu-Bonin, J. Geophys. Res., 103, B7, 15015-15036, 1998.

Tajima, F., Y. Fukao, M. Obayashi, and T. Sakurai, Evaluation of slab images in the northwestern Pacific, Special issue of the Ocean Hemisphere Project symposium, Earth Planet. Space, 50, no. 11 and 12, 953-964, 1998.

van der Hilst, R.D., R. Engdahl, W. Sparkman, and G. Nolet, Tomographic imaging of subducted lithosphere below northwest Pacific islands arcs, Nature, 353, 37-43, 1991.

Chapter 12

Appendices